論文 / 著書情報
Article / Book Information

Title	New spectra of responses and control force for design of equivalent-input-disturbance-based active structural control of base-isolated buildings
Authors	Kou Miyamoto, Daiki Sato, Jinhua She, Yinli Chen, Qing-Long Han
Citation	Journal of Sound and Vibration, Vol. 507,
Pub. date	2021, 9
DOI	https://dx.doi.org/10.1016/j.jsv.2021.116160
Creative Commons	See next page.
Note	This file is author (final) version.

License

New spectra of responses and control force for design of equivalent-input-disturbance-based active structural control of base-isolated buildings

Kou Miyamoto[a,*], Daiki Sato[b], Jinhua She[c], Yinli Chen[d], Qing-Long Han[e]

[a]*Institute of Technology, Shimizu Corporation, Koto, Tokyo 135-0044, Japan*
[b]*FIRST, Tokyo Institute of Technology, Yokohama, Kanagawa 226-8503, Japan*
[c]*Department of Mechanical engineering, Tokyo University of Technology, Hachioji, Tokyo 192-0982, Japan*
[d]*Department of Architecture and Building Engineering, Tokyo Institute of Technology, Yokohama, Kanagawa 226-8503, Japan*
[e]*School of Software and Electrical Engineering, Swinburne University of Technology, Victoria 3122, Australia*

Abstract

This paper presents new spectra of responses and control force for an active base-isolated building that uses the equivalent-input-disturbance (EID) approach for active structural control. The EID approach estimates the effect of disturbances and uses it to suppress building vibrations. This system plugs an EID estimator into a conventional state-feedback control system. Note that these kinds of disturbance-rejection systems contain both feedforward and feedback terms from disturbances to a control output. This paper describes spectra that can handle systems with such structure. The spectra can be used to simplify the design of an active structural control system. This paper illustrates the use of the spectra for control-system design and presents a design algorithm for the EID-based control system. A shear building model and 44 kinds of earthquake waves are used to demonstrate the availability of the spectra.

Keywords: equivalent input disturbance (EID), active structural control, response spectrum, control-force spectrum, feedforward control, feedback control

1. Introduction

Base isolation has been widely used in buildings to protect people and household effects from earthquakes since the 1995 Kobe earthquake in Japan [1]. Recently, strategies of active structural control, which combine control and structural engineering, have also been extensively studied and applied to improve control performance. Most of control systems that used the PID control [2], the linear quadratic regulator (LQR) [3, 4, 5], and the computational-intelligence-based control for control-system design [6, 7]. Note that there is a trade-off between disturbance-rejection performance and other control performance in those control systems. This problem can be solved by using a control-system configuration that contains a disturbance-estimation mechanism. This system enables the independent design of input-output and disturbance-rejection characteristics.

Many methods have been proposed to estimate disturbances, for example, adaptive disturbance estimation [8], the active disturbance-rejection control (ADRC) [9, 10], and the equivalent-input-disturbance (EID) approach [11]. The ADRC and EID methods have faster and more satisfactory disturbance-rejection performance than adaptive control does. A comparison between the ADRC and EID methods reveals that the EID approach has a much-relaxed requirement on a disturbance than the ADRC method does, that is, the EID approach does not require $\lim_{t\to\infty} \dot{d}(t) = 0$. Moreover, the EID approach can be applied to a non-square plant (the numbers of the inputs and outputs are not the same). This point is also important in active structural control because the number of the outputs is usually larger than that of the inputs of a structure.

The application of the EID approach in structural control shows that the method greatly improves disturbance-rejection (that is, vibration-suppression) performance in a low-frequency band [4, 12]. Since low-frequency signals

*Corresponding author. *E-mail address:* kou_miyamoto@shimz.co.jp (K. Miyamoto).

give a large influence on base-isolated buildings due to their long natural periods, this method is particularly suitable for structural control. The EID approach was extended to suppress both the displacement and the absolute acceleration of a building [13].

Since an EID-based control system includes four parts: a building, a feedback controller, a low-pass filter, and an observer; gains of the feedback and observer and parameters of the low-pass filter need to be tuned in control system design. However, the parameters are usually determined by experience or trial and error. Furthermore, the maximum control force, displacement, absolute acceleration, and other system responses are not the same for different earthquake waves. Thus, how to guarantee required control specifications for all possible earthquake waves is important for system design.

The response spectrum method is used to design a passive structural-control system [14]. This method is based on the responses of a single-degree-of-freedom model for an earthquake wave and estimates the peak value of the displacement, velocity, and absolute acceleration of a structure. The use of the peak value of responses makes the method easy to use. Note that the base-isolated floor of a passive-base-isolated building is much softer than the superstructure. Such a building can be described as a single-degree-of-freedom model because the influence of the first mode is much bigger than that of the other modes [15]. This makes the method possible to design a passive base-isolated building control system [16, 14]. Sato et al. presented a new spectrum, called the control force spectrum, that estimates the maximum control force and extended the response spectrum method to design an active base-isolated building control system [17].

This study extended the control force spectrum to deal with an EID-based structural-control system. Since an EID-based structural-control system has both feedforward and feedback terms from disturbances to a control output, we derive a new control-force spectrum for such a system. Making use of the spectra simplifies the design of a structural control system. We present a new design algorithm based on the spectra for the EID-based structural-control system to illustrate this feature of the spectra. 44 earthquake waves selected from the Federal Emergency Management Agency (FEMA) P695 [18] were used to design an active structural control system for a shear building to demonstrate the availability of the spectra.

Notation: $\{1\}$ is a vector with all entries being one, $X(s)$ is the Laplace transform of $x(t)$, $\mathrm{avg}[x(t)]$ is the average of $x(t)$, $\mathrm{std}[x(t)]$ is the standard deviation of $x(t)$.

2. EID-based structural-control system for base-isolated buildings

The equation of motion of an n-degree-of-freedom shear building with active structural control, which is called a plant hereafter, is described by

$$M_S\ddot{x}(t) + D_S\dot{x}(t) + K_S x(t) = -M_S\{1\}\ddot{x}_g(t) + E_u u(t), \tag{1}$$

where M_S ($\in \mathbb{R}^{n\times n}$) is a mass matrix, D_S ($\in \mathbb{R}^{n\times n}$) is a damping matrix, K_S ($\in \mathbb{R}^{n\times n}$) is a stiffness matrix, E_u ($\in \mathbb{R}^n$) is a matrix that indicates the placement of active structural control devices, $u(t)$ ($\in \mathbb{R}$) is a control force, $x(t)$ ($\in \mathbb{R}^n$) is a relative displacements vector, and $\ddot{x}_g(t)$ ($\in \mathbb{R}$) is ground acceleration.

Note that the absolute acceleration of a building is given by regrouping (1)

$$\ddot{x}(t) + \{1\}\ddot{x}_g(t) = -M_S^{-1}K_S x(t) - M_S^{-1}D_S\dot{x}(t) + M_S^{-1}E_u u(t). \tag{2}$$

The state-space representation of the plant is (Fig.1)

$$\begin{cases} \dot{z}(t) = Az(t) + Bu(t) + B_d\ddot{x}_g(t), \\ y(t) = Cz(t) + Du(t), \end{cases} \tag{3}$$

where

$$\begin{cases} z(t) = \begin{bmatrix} x(t) \\ \dot{x}(t) \end{bmatrix}, \quad A = \begin{bmatrix} 0 & I \\ -M_S^{-1}K_S & -M_S^{-1}D_S \end{bmatrix}, \\ B_d = -\begin{bmatrix} 0 \\ \{1\} \end{bmatrix}, \quad B = \begin{bmatrix} B_1 \\ B_2 \end{bmatrix}, \quad B_1 = 0, \quad B_2 = M_S^{-1}E_u, \end{cases} \tag{4}$$

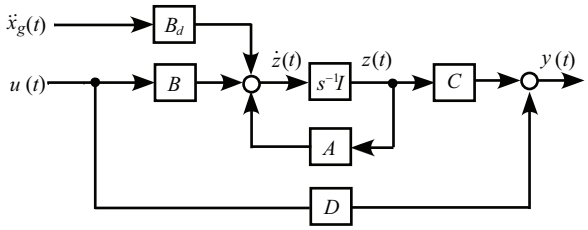

Fig. 1: Plant with its output being absolute acceleration.

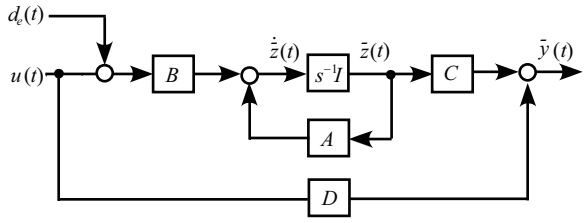

Fig. 2: Plant with EID.

where $z(t)$ is the state of the plant, A is a system matrix that determines the dynamic characteristics of the system, B is a control input matrix, and B_d is a disturbance input matrix. For the output $y(t)$, if we take it to be the placement,

$$C = \begin{bmatrix} I & 0 \end{bmatrix}, \quad D = 0; \tag{5}$$

the velocity,

$$C = \begin{bmatrix} 0 & I \end{bmatrix}, \quad D = 0; \tag{6}$$

and the absolute acceleration,

$$C = \begin{bmatrix} -M_S^{-1}K_S & -M_S^{-1}D_S \end{bmatrix}, \quad D = M_S^{-1}E_u. \tag{7}$$

The plant is called a strictly proper system if $D = 0$, and a proper system if $D \neq 0$.

Without loss of generality, the following assumption is made for the plant:

Assumption 1. *Plant* (A, B, C) *is controllable and observable.*

On the other hand, let the plant have a disturbance on the control input channel (Fig. 2):

$$\begin{cases} \dot{\bar{z}}(t) = A\bar{z}(t) + B[u(t) + d_e(t)], \\ \bar{y}(t) = C\bar{z}(t) + Du(t). \end{cases} \tag{8}$$

An EID is defined as follows [11]:

Definition 1. *If* $\bar{y}(t)$ *in (8) equals* $y(t)$ *in (3) for all* $t \geq 0$*, then* $d_e(t)$ *is called an EID of the original disturbance,* $\ddot{x}_g(t)$*.*

It is clear from the definition of an EID that an EID is a signal on the control-input channel that has the same effect on the output as the original disturbance does.

An EID-based structural-control system (Fig. 3) contains an EID estimator that uses a low-pass filter, $F(s)$, to process the information of the state observer. B^+ in Fig. 3 is the pseudo-inverse matrix of B:

$$B^+ = \left(B^{\mathsf{T}}B\right)^{-1} B^{\mathsf{T}}. \tag{9}$$

The state observer of the plant is

$$\begin{cases} \dot{\hat{z}}(t) = A\hat{z}(t) + Bu(t) + L_P[y(t) - \hat{y}(t)], \\ \hat{y}(t) = C\hat{z}(t) + Du(t), \end{cases} \tag{10}$$

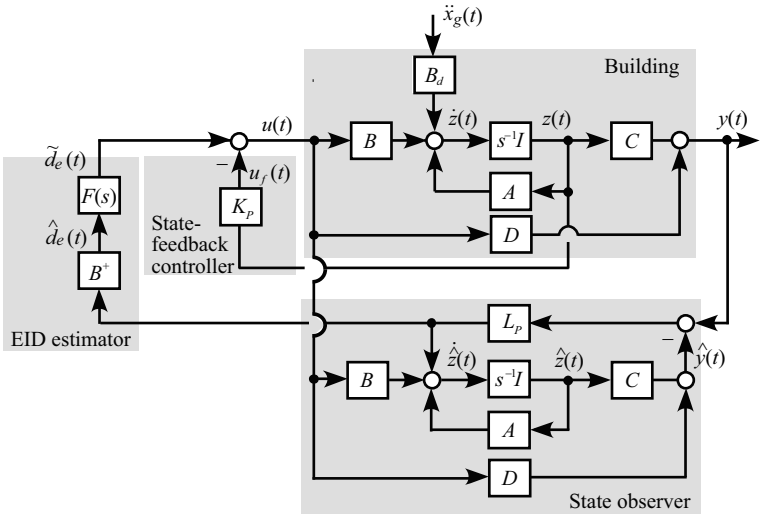

Fig. 3: Configuration of EID-based structural-control system.

where L_P is an observer gain, $\hat{z}(t)$ and $\hat{y}(t)$ are the state and the output of the state observer. Letting

$$\Delta z(t) = z(t) - \hat{z}(t) \tag{11}$$

and combining (8) and (10) yield

$$\begin{cases} \Delta\dot{z}(t) = (A - L_P C)\Delta z(t) + B d_e(t), \\ \Delta y(t) = C\Delta z(t). \end{cases} \tag{12}$$

An estimate of the EID, $\hat{d}_e(t)$, is [11]

$$\hat{d}_e(t) = B^+ L_P C \Delta z(t). \tag{13}$$

$F(s)$ is used to select the angular-frequency band for disturbance rejection and adjust the control force. This study used the following low-pass filter:

$$F(s) = \frac{N_F}{T_F s + 1}, \quad T_F \leq \frac{1}{5\omega_m}, \tag{14}$$

where T_F is the time constant of $F(s)$, which is used to select the frequency band for disturbance rejection; N_F ($0 < N_F \leq 1$) is a gain of the filter, which is used to adjust the maximum control force [5]; and ω_m is the largest angular frequency for disturbance estimation and rejection. The filtered estimate of the EID is

$$\tilde{D}_e(s) = F(s)\hat{D}_e(s), \tag{15}$$

where $\tilde{D}_e(s)$ and $\hat{D}_e(s)$ are the Laplace transforms of $\tilde{d}_e(t)$ and $\hat{d}_e(t)$, respectively.

The control force combines the feedback control force, $u_f(t)$, and the estimated EID, $\tilde{d}_e(t)$

$$u(t) = u_f(t) - \tilde{d}_e(t). \tag{16}$$

The control law of the feedback control is

$$u_f(t) = K_P z(t), \tag{17}$$

where K_P is the gain of the state-feedback controller, and it is

$$K_P = \begin{bmatrix} K_{P1} & K_{P2} \end{bmatrix}. \tag{18}$$

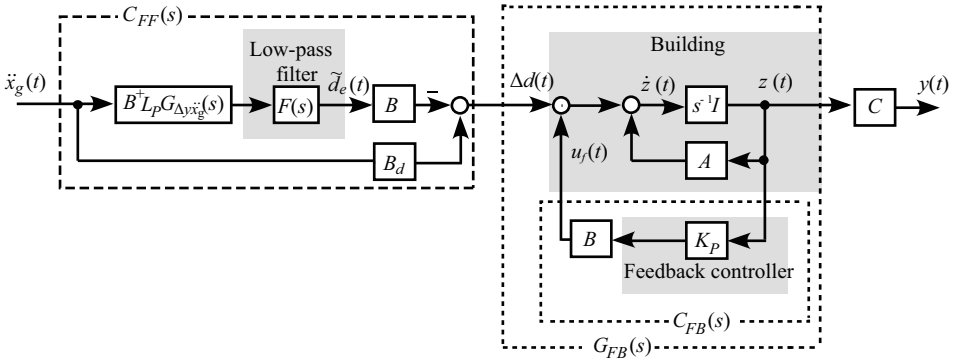

Fig. 4: Control system from ground acceleration to displacement or velocity.

3. Description of disturbance response

To induce new spectra, this section first derives the relationship between the disturbance and the output of the system. Since the disturbance influence on the absolute acceleration is quite different from that on the displacement or velocity, they are discussed separately.

3.1. Disturbance influence on displacement and velocity

Redrawing Fig. 3 using (12), (13), (15), (16), and (17) yields Fig. 4 that shows the block diagram from the input of an earthquake wave to the displacement or velocity. The control system has two controllers: feedforward [$C_{FF}(s)$] and feedback [$C_{FB}(s)$]

$$\begin{cases} C_{FF}(s) = B_d - BG_{\tilde{d}_e\ddot{x}_g}(s), \\ C_{FB}(s) = K_P B, \end{cases} \tag{19}$$

where

$$G_{\tilde{d}_e\ddot{x}_g}(s) = F(s)B^+L_PG_{\Delta y\ddot{x}_g}(s) \tag{20}$$

$$G_{\Delta y\ddot{x}_g}(s) = C\left[sI - (A - L_PC)\right]^{-1}B_d. \tag{21}$$

The derivation of $C_{FF}(s)$ is given in Appendix A.

The transfer function from an earthquake wave, $\ddot{x}_g(t)$, to the output (displacement or velocity), $y(t)$ (Fig. 4) is

$$G_{y\ddot{x}_g}(s) = CG_{FB}(s)C_{FF}(s), \tag{22}$$

where

$$G_{FB}(s) = \left[sI - (A + BK_P)\right]^{-1}. \tag{23}$$

Note that C in (22) is given by (5) for the displacement and (6) for the velocity.

3.2. Disturbance influence on absolute acceleration

Combining (1), (16), (17) and (18) gives

$$\ddot{x}(t) + \{1\}\ddot{x}_g(t) \quad := \quad y_{FB}(t) - \ddot{x}_{EID}(t), \tag{24}$$

where

$$y_{FB}(t) = C_Az(t), \tag{25}$$

$$\ddot{x}_{EID}(t) = B_2\tilde{d}_e(t), \tag{26}$$

$$C_A = \begin{bmatrix} -M_S^{-1}K_{Seq} & -M_S^{-1}D_{Seq} \end{bmatrix}, \tag{27}$$

$$K_{Seq} = K_S - E_uK_{P1},\ D_{Seq} = D_S - E_uK_{P2}, \tag{28}$$

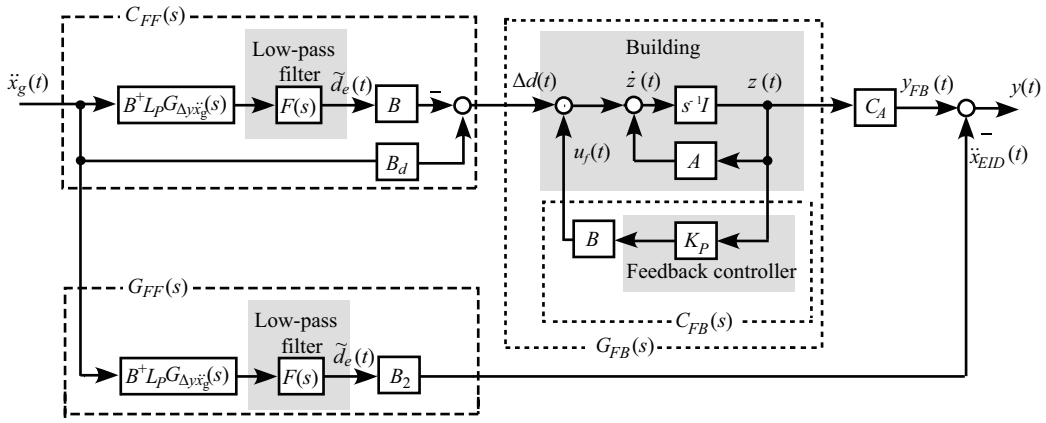

Fig. 5: Control system from ground acceleration to absolute acceleration.

where B_2 is given in (4); and K_{Seq} and D_{Seq} are the stiffness and damping matrices with active structural control, respectively, C_A is the output matrix for the absolute acceleration with a feedback controller, and $\ddot{x}_{EID}(t)$ is the acceleration caused by using the feedforward controller.

$$\begin{aligned} y_{FB}(t) &= C_A z(t) \\ &= \mathcal{L}^{-1}\left[C_A G_{FB}(s) C_{FF}(s) \cdot \ddot{X}_g(s)\right], \end{aligned} \tag{29}$$

where $\mathcal{L}^{-1}$ is an inverse Laplace transform. And combining (20) and (26) gives

$$\ddot{x}_{EID}(t) = B_2 \tilde{d}_e(t) \tag{30}$$

$$= \mathcal{L}^{-1}\left[B_2 G_{\tilde{d}_e \ddot{x}_g}(s) \cdot \ddot{X}_g(s)\right]. \tag{31}$$

Substituting (31) and (29) into (24) yields

$$\begin{aligned} \ddot{x}(t) + \{1\}\,\ddot{x}_g(t) &= \mathcal{L}^{-1}\left[C_A G_{FB}(s) G_{FF}(s) \cdot \ddot{X}_g(s)\right] - \mathcal{L}^{-1}\left[B_2 G_{\tilde{d}_e \ddot{x}_g}(s) \cdot \ddot{X}_g(s)\right] \\ &= \mathcal{L}^{-1}\left\{\left[C_A G_{FB}(s) G_{FF}(s) - B_2 G_{\tilde{d}_e \ddot{x}_g}(s)\right] \cdot \ddot{X}_g(s)\right\}. \end{aligned} \tag{32}$$

Therefore, the transfer function from the disturbance to the absolute acceleration is (Fig. 5)

$$\begin{aligned} G_{(\ddot{x}+\{1\}\ddot{x}_g)\ddot{x}_g}(s) &= \left[\ddot{X}(s) + \{1\}\,\ddot{X}_g(s)\right] \ddot{X}_g^{-1}(s) \\ &= C_A G_{FB}(s) G_{FF} - B_2 G_{\tilde{d}_e \ddot{x}_g}(s). \end{aligned} \tag{33}$$

Note that $BG_{\tilde{d}_e \ddot{x}_g}(s) = \begin{bmatrix} 0 \\ B_2 G_{\tilde{d}_e \ddot{x}_g}(s) \end{bmatrix}$.

Since the EID-based structural-control system contains both the feedback and feedforward controller, we need to consider the influence of the feedforward part on the absolute acceleration.

4. Spectra of responses and control force and control-system design

This section explains new spectra for the EID-based structural-control system. Since the influence of the first mode is much bigger than that of the others for a base-isolated building, such a building can be modeled as a single-degree-of-freedom system (Fig. 6), that is, $n = 1$ and $E_u = 1$. On the other hand, The dynamics of the building without active structural control is

$$M_s \ddot{x}_{na}(t) + D_S \dot{x}_{na}(t) + K_S x_{na}(t) = -M_S \ddot{x}_g(t), \tag{34}$$

where $x_{na}(t)$ is the displacement of the plant.

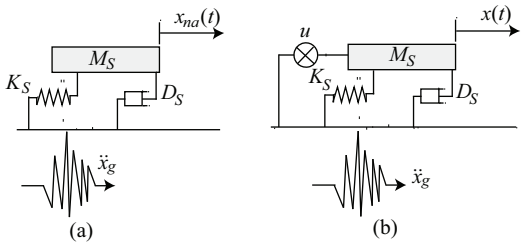

Fig. 6: Single-degree-of-freedom model: (a) without active structural control and (b) with active structural control.

4.1. Spectra of responses and control force for velocity feedback control

The response-spectrum method estimates the maximum displacement, velocity, and absolute acceleration of the plant (34). These spectra are called displacement-response spectrum $[S_D(\omega_S, h_S, \ddot{x}_g)]$, velocity-response spectrum $[S_V(\omega_S, h_S, \ddot{x}_g)]$ and the absolute-acceleration-response spectrum $[S_A(\omega_S, h_S, \ddot{x}_g)]$

$$|x_{na}(t)|_{\max} = S_D\left(\omega_S, h_S, \ddot{x}_g\right), \tag{35}$$

$$|\dot{x}_{na}(t)|_{\max} = S_V\left(\omega_S, h_S, \ddot{x}_g\right), \tag{36}$$

$$|\ddot{x}_{na}(t) + \ddot{x}_g(t)|_{\max} = S_A\left(\omega_S, h_S, \ddot{x}_g\right), \tag{37}$$

where ω_S is the natural angular frequency, and h_S is the damping ratio of the plant and

$$\begin{cases} \omega_S \approx \left(M_S^{-1}K_S\right)^{1/2}, \\ h_S = D_S(2M_S\omega_S)^{-1}. \end{cases} \tag{38}$$

Sato et al. extended these spectra for the design of active base-isolated buildings for velocity-feedback control [17]:

$$u(t) = K_P\dot{x}(t). \tag{39}$$

Substituting (39) into (1) yields

$$M_S\ddot{x}(t) + D_{Seq}\dot{x}(t) + K_S x(t) = -M_S\ddot{x}_g(t), \tag{40}$$

where D_{Seq} is an equivalent damping coefficient given by

$$D_{Seq} = D_S + K_P. \tag{41}$$

The damping ratio of the building with the velocity-feedback controller is

$$\begin{cases} h_{Seq} = h_S + h_{KP}, \\ h_{KP} = K_P(2M_S\omega_S)^{-1}, \end{cases} \tag{42}$$

where h_S is the initial damping ratio and h_{KP} is an added damping ratio by velocity-feedback control. This equation shows that the velocity-feedback controller improves the damping ratio of the system. Thus, the natural frequency of the control system can be estimated using (38). As a result, the maximum displacement, velocity, and the absolute acceleration are estimated by following spectra:

$$|x(t)|_{\max} = S_D\left(\omega_S, h_{Seq}, \ddot{x}_g\right), \tag{43}$$

$$|\dot{x}(t)|_{\max} = S_V\left(\omega_S, h_{Seq}, \ddot{x}_g\right), \tag{44}$$

$$|\ddot{x}(t) + \ddot{x}_g(t)|_{\max} = S_A\left(\omega_S, h_{Seq}, \ddot{x}_g\right). \tag{45}$$

Since the control force is given by (39), the maximum control force, $|u(t)|_{\max}$, is estimated by the maximum velocity response:

$$\begin{aligned} |u(t)|_{\max} &= K_P |\dot{x}(t)|_{\max} \\ &= K_P S_V\left(\omega_S, h_{Seq}, \ddot{x}_g\right). \end{aligned} \tag{46}$$

A control-force spectrum, $U\left(\omega_S, h_{Seq}, \ddot{x}_g\right)$, that estimates the maximum control force is defined to be

$$U\left(\omega_S, h_{Seq}, \ddot{x}_g\right) = K_P S_V\left(\omega_S, h_{Seq}, \ddot{x}_g\right). \tag{47}$$

Sato et al. presented a normalized control force spectrum [17]

$$\begin{aligned} C_U\left(\omega_S, h_{Seq}, \ddot{x}_g\right) &= \frac{K_P S_V\left(\omega_S, h_{Seq}, \ddot{x}_g\right)}{M_S g} \\ &= \frac{U\left(\omega_S, h_{Seq}, \ddot{x}_g\right)}{M_S g}, \end{aligned} \tag{48}$$

where g is the gravitational acceleration. This spectrum means the shear-force coefficient of the control force, which is the ratio of the maximum control force to the weight of the building. Since the first natural period of a base-isolated building is usually much longer than a time delay caused by information transmission, control-law calculation, etc. in a system, the effect of a time delay is small.

4.2. Spectra for EID-based structural-control system

The Laplace transform of the residual disturbance (Fig. 4) is

$$\Delta D(s) = C_{FF}(s)\ddot{X}_g(s), \tag{49}$$

which is the input to $G_{FB}(s)$, EID-based structural-control system. Therefore, the maximum displacement and the velocity of EID-based structural-control system can be estimated using the response spectra for $\Delta d(t)$. This gives the displacement and velocity response spectra for the EID-based structural-control system

$$S_{D,EID}\left(\omega_S, h_{Seq}, \ddot{x}_g\right) = S_D\left(\omega_S, h_{Seq}, \Delta d\right), \tag{50}$$

$$S_{V,EID}\left(\omega_S, h_{Seq}, \ddot{x}_g\right) = S_V\left(\omega_S, h_{Seq}, \Delta d\right). \tag{51}$$

Note that the relationship between $S_A\left(\omega_S, h_{Seq}, \ddot{x}_g\right)$ and $S_V\left(\omega_S, h_{Seq}, \ddot{x}_g\right)$ is

$$S_A\left(\omega_S, h_{Seq}, \ddot{x}_g\right) \approx \omega_S S_V\left(\omega_S, h_{Seq}, \ddot{x}_g\right). \tag{52}$$

That is, the absolute acceleration of the feedback control system is

$$|y_{FB}(t)|_{\max} \approx \omega_S S_{V,EID}\left(\omega_S, h_{Seq}, \Delta d\right). \tag{53}$$

It is clear from (24) and Fig. 5 that the absolute acceleration is the sum of the feedback control part, $y_{FB}(t)$ and the feedforward control part, $\ddot{x}_{EID}(t)$. $y_{FB}(t)$ given in (53) is not enough to estimate the absolute acceleration of the EID-based structural-control system.

In this study, we estimated the maximum absolute acceleration of the EID-based structural-control system by using the combination of the absolute sum (ABS) and the root sum of squares (RSS) of the maximum $y_{FB}(t)$ and $\ddot{x}_{EID}(t)$.

First, we calculate the maximum $\ddot{x}_{EID}(t)$. The dynamics of the building with (39) for the EID, $d_e(t)$, is

$$M_S \ddot{\bar{x}}(t) + D_{Seq}\dot{\bar{x}}(t) + K_S \bar{x}(t) = -d_e(t), \tag{54}$$

where $\bar{x}(t)$ is the displacement of a building. Since the response caused by the EID is the same as the original disturbance does, the following relationship holds for (40) and (54):

$$x(t) = \bar{x}(t). \tag{55}$$

Comparing (40) and (54) yields

$$M_S \ddot{x}_g(t) = d_e(t). \tag{56}$$

$\tilde{d}_e(t)$ is a filtered estimate of the EID for $\omega \in [0, \omega_m]$. Thus, the following is true from (14) and (56):

$$\tilde{d}_e(t) \approx N_F d_e(t) = N_F M_S \ddot{x}_g(t). \tag{57}$$

Substituting (57) and B_2 in (4) into (26) yields

$$\ddot{x}_{EID}(t) = B_2 \tilde{d}_e \approx N_F \ddot{x}_g(t). \tag{58}$$

It is clear from the above equation, (58), that the system estimates the EID appropriately in the prescribed frequency range for disturbance estimation and the transfer function $B_2 G_{\tilde{d}_e \ddot{x}_g}(s)$ is approximated by N_F.

We define the absolute acceleration spectrum for the EID-based structural-control system to be

$$S_{A,EID}\left(\omega_S, h_{S\,eq}, \ddot{x}_g\right) = \frac{\mathrm{ABS}_{\mathrm{ACC}} + \mathrm{RSS}_{\mathrm{ACC}}}{2}, \tag{59}$$

where

$$\mathrm{ABS}_{\mathrm{ACC}} = N_F |\ddot{x}_g(t)|_{\max} + \omega_S S_{V,EID}\left(\omega_S, h_{S\,eq}, \Delta d\right), \tag{60}$$

$$\mathrm{RSS}_{\mathrm{ACC}} = \sqrt{\left[N_F |\ddot{x}_g(t)|_{\max}\right]^2 + \left[\omega_S S_{V,EID}\left(\omega_S, h_{S\,eq}, \Delta d\right)\right]^2}. \tag{61}$$

The control force is the combination of the feedback control force, $u_f(t)$, and the estimated EID, $\tilde{d}_e(t)$:

$$u(t) = u_f(t) - \tilde{d}_e(t). \tag{62}$$

The control force spectrum is defined to be

$$U_{EID}\left(\omega_S, h_{S\,eq}, \ddot{x}_g\right) = \frac{\mathrm{ABS}_{\mathrm{U}} + \mathrm{RSS}_{\mathrm{U}}}{2}, \tag{63}$$

where

$$\begin{aligned} \mathrm{ABS}_{\mathrm{U}} &= |u_f|_{\max} + |\tilde{d}_e(t)|_{\max} \\ &= K_P S_V\left(\omega_S, h_{S\,eq}, \ddot{x}_g\right) + N_F |M_S \ddot{x}_g(t)|_{\max} \end{aligned} \tag{64}$$

$$\begin{aligned} \mathrm{RSS}_{\mathrm{U}} &= \sqrt{|u_f|^2_{\max} + |\tilde{d}_e(t)|^2_{\max}} \\ &= \sqrt{\left[K_P S_V\left(\omega_S, h_{S\,eq}, \ddot{x}_g\right)\right]^2 + \left[N_F |M_S \ddot{x}_g(t)|_{\max}\right]^2}. \end{aligned} \tag{65}$$

The normalized control-force spectrum for an EID-based structural-control system is

$$C_{U,EID}\left(\omega_S, h_{S\,eq}, \ddot{x}_g\right) = \frac{U_{EID}\left(\omega_S, h_{S\,eq}, \ddot{x}_g\right)}{M_S g}. \tag{66}$$

The characteristics of the active structural control system are clearly described by the spectra (50), (51), (59), and (63). Thus, a system designed based on those spectra has satisfactory control performance. The next subsection explains how those spectra are used in the system design.

4.3. Design of EID-based structural-control system

The EID-based structural-control system consists of the feedback and feedforward control systems. Velocity-feedback control adjusts the damping ratio of the system.

The feedback controller, K_P, is designed based on prescribed control specifications and the observer gain, L_P, is designed using the pole placement method.

For a selected h_{Seq}, the gain of the state-feedback controller is given by

$$K_P = \begin{bmatrix} 0 & -D_{Seq} + D_S \end{bmatrix} = \begin{bmatrix} 0 & -2M_S\omega_S(h_{Seq} - h_S) \end{bmatrix}. \tag{67}$$

Remark 1. *Note that the controller gain (67) is equivalent to the gain that is designed by minimizing the following performance index [17]*

$$J = \int_0^\infty \left\{ z^\mathsf{T}(t)Qz(t) + u^\mathsf{T}(t)Ru(t) \right\} dt, \tag{68}$$

where

$$Q = \begin{bmatrix} 0 & 0 \\ 0 & D_{Seq} - D_S \end{bmatrix}, \; R = 1 \tag{69}$$

are the weighting matrices for the state and the control force, respectively. The gain of the state-feedback controller is

$$K_P = -R^{-1}B^\mathsf{T}P, \tag{70}$$

where P is the solution of the following Riccati equation:

$$A^\mathsf{T}P + PA - PBR^{-1}B^\mathsf{T}P + Q = 0. \tag{71}$$

Ackerman's formula is used in the pole placement method to design the observer gain, L_P. More specifically, for selected eigenvalues of $A - L_P C_o$, $a_o \pm jb_o$, and the output matrix $C_o = \begin{bmatrix} C_{o1} & C_{o2} \end{bmatrix}$, the observer gain is given by

$$L_P = \left[\begin{bmatrix} 0 & 1 \end{bmatrix} U_C^{-1} \Phi \right]^\mathsf{T}, \tag{72}$$

where

$$U_C^{-1} = \begin{bmatrix} C_o^\mathsf{T} & A^\mathsf{T}C_o^\mathsf{T} \end{bmatrix} \tag{73}$$

$$\Phi = \left[A^2 - 2a_o A + (a_o^2 + b_o^2)I \right]^\mathsf{T}. \tag{74}$$

For $C_{o1} = -K_S/M_S$ and $C_{o2} = -D_S/M_S$, L_P is

$$L_P = \begin{bmatrix} L_{P1} \\ L_{P2} \end{bmatrix} = \begin{bmatrix} \dfrac{f_o}{\pi f_u^2}\left(\dfrac{f_o h_S}{f_u} - h_o \right) \\ 1 - \dfrac{\pi f_o^2}{f_u} \end{bmatrix}, \tag{75}$$

where f_u $(= 1/T_u)$ is the natural frequency of the building model; and f_o and h_o are the natural frequency and the damping ratio of the observer, respectively.

4.4. Design algorithm of EID control system

We condense the above discussion into a system design algorithm.

Algorithm of designing EID-based structural-control system

Step 1: set the limitation of the maximum displacement (x_{lim}) and the limitation of the maximum shear force of the control force (u_{lim}/mg) for a model with the natural period (T_u) and the damping ratio of the structure (h_S).

Step 2: Choose a set of earthquake waves, $\{\ddot{x}_g\}$; and a candidate set of equivalent damping ratios, $\{h_{Seq}\}$.

Step 3: Calculate the velocity-feedback controller using (67).

Step 4: Choose the parameters of the low-pass filter, T_F based on ω_m that is usually determined taking into consideration of the natural frequency of the building and the dominant components of $\{\ddot{x}_g\}$. And choose an N_F.

Step 5: Calculate the observer gain, L_P, using (75), and choose f_o and h_o such that $|B_2 G_{\tilde{d}_e \ddot{x}_g}(j\omega)| \approx N_F$ holds around the dominant frequencies of the earthquake waves given in Step 2. Check the frequency response of $B_2 G_{\tilde{d}_e \ddot{x}_g}(s)$ for all the pairs of f_o and h_o.

Step 6: Check the responses and the shear force of the EID-based structural-control system using the spectra, $S_{D,EID}\left(\omega_S, h_{Seq}, \ddot{x}_g\right)$, $S_{V,EID}\left(\omega_S, h_{Seq}, \ddot{x}_g\right)$, $S_{A,EID}\left(\omega_S, h_{Seq}, \ddot{x}_g\right)$, and $C_{U,EID}\left(\omega_S, h_{Seq}, \ddot{x}_g\right)$. Adjust the equivalent damping ratio, h_{Seq}, and the low-pass filter gain, N_F, to ensure that the maximum displacement and the maximum shear force of the control force are smaller than the given limitations.

Step 7: Check if the maximum response and shear force satisfy the limitations, if all the spectra are satisfactory, and if $\tilde{d}_e(t)$ is adequate. If not, go to Step 3; otherwise, finish.

5. Numerical verification

This section first verifies the effectiveness of the new spectra. Then, it uses an example to show the design procedure based on the spectra.

5.1. Validity of new spectra

Consider a single-degree-of-freedom model:

- Mass of the model: $M_S = 100$
- Damping ratio of the structure: $h_S = 0.02$
- The natural period of the structure: $T_u = 0.5 \sim 10.0$ s.

Note that the natural period of a base-isolated building is usually very long. However, this example uses a natural period that covers a wide range to analyze the characteristics of the spectra.

For an EID-based structural-control system with the following parameters

- Equivalent damping ratio of the feedback control system: $h_{Seq} = 0.4$
- Time constant of the low-pass filter: $T_F = 0.01$ s
- Gain of the low-pass filter: $N_F = 0.5$
- Natural frequency of the observer: $f_o = 10$ Hz
- Damping ratio of the observer: $h_o = 0.8$,

we carried out the time-history analyses and showed $S_{A,EID}\left(\omega_S, h_{Seq}, \ddot{x}_g\right)$ [Fig. 8 (a)], $C_{U,EID}\left(\omega_S, h_{Seq}, \ddot{x}_g\right)$ [Fig. 8 (b)], $S_{D,EID}\left(\omega_S, h_{Seq}, \ddot{x}_g\right)$ [Fig. 8 (c)], and $S_{V,EID}\left(\omega_S, h_{Seq}, \ddot{x}_g\right)$ [Fig. 8 (d)] for 44 earthquake. (Tabs 1 and 2). These waves were recommended for the evaluation of vibration-suppression performance by the Federal Emergency Management Agency (FEMA) P695 [18]. The velocity response spectra for 5% damping ratio and the average of the 44 waves are shown in Fig. 7. Moreover, velocity-response spectra for a structure with a 5% damping ratio are shown in Appendix B (Figs. B.19-B.40).

Figure 8 (a) and (b) show that the presented method satisfactorily estimated the maximum absolute acceleration and the maximum shear force of the control force for $T_u = 0.5 \sim 5.0$ s, but the errors between the estimates and analysis results are large for $T_u = 5.5 \sim 10.0$ s. The reason is explained as follows. The frequency response of $B_2 G_{\tilde{d}_e \ddot{x}_g}(s)$ (Fig. 9) shows that the gain for $T_u = 10.0$ s is more than two times larger than 0.5 (the peak value is 1.1) during the frequency range $[1, 10]$ Hz. The gain estrangement from the designed value 0.5 in the frequency band caused such errors.

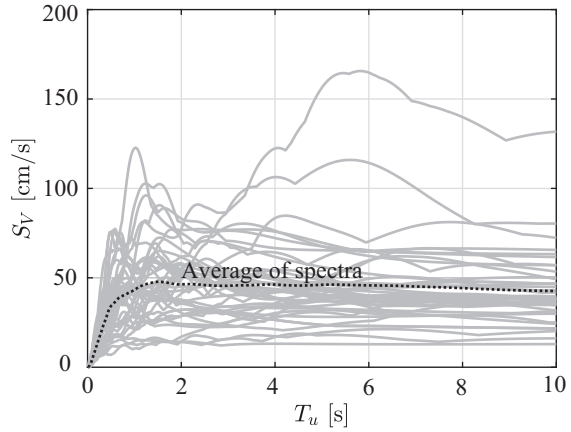

Fig. 7: Velocity response spectra (h = 5%) for waves and average of them.

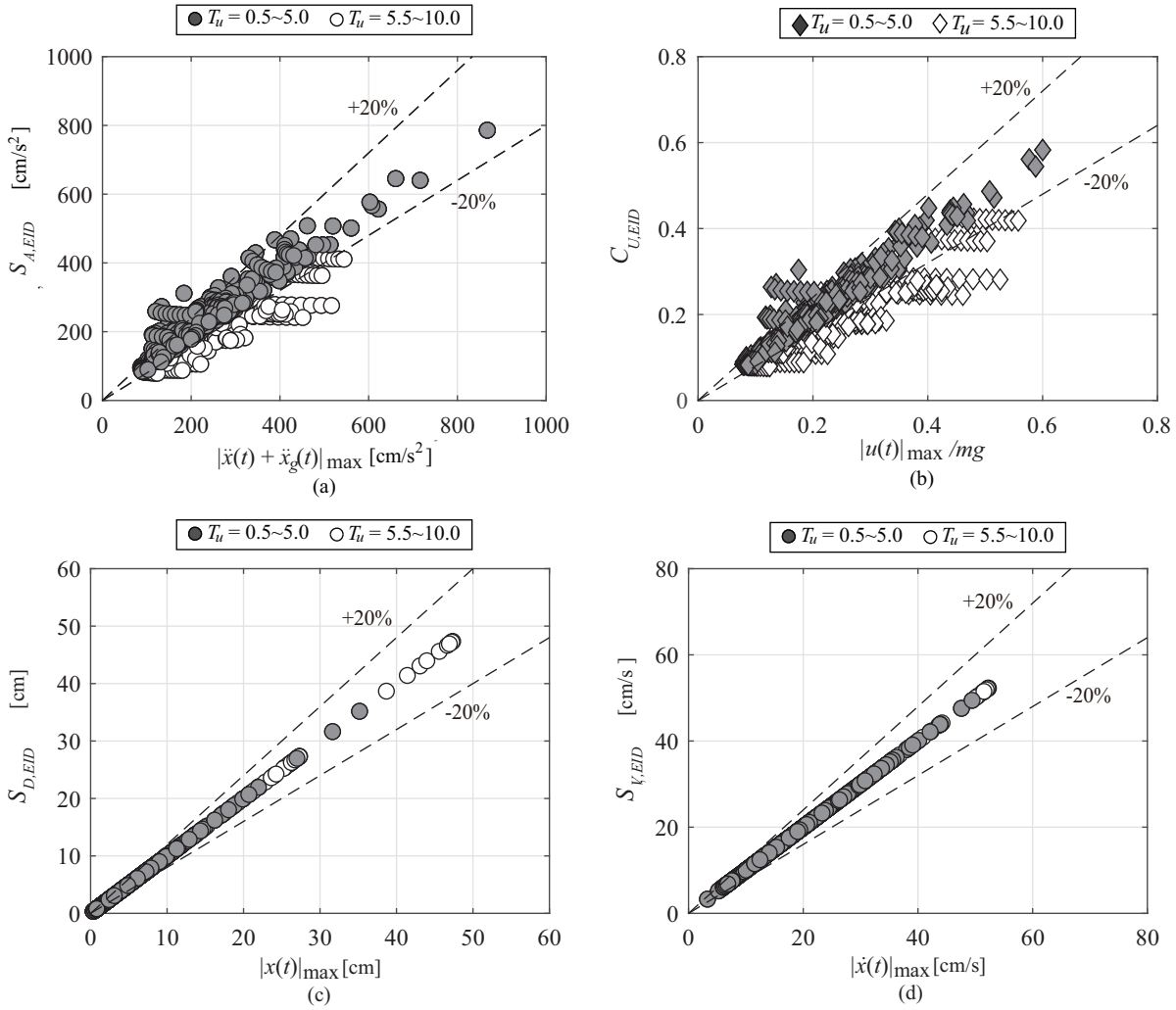

Fig. 8: Estimation vs. analysis for (a) maximum absolute acceleration, (b) maximum C_U (N_F = 0.5), (c) displacement, and (d) velocity for f_o = 10 Hz.

Table 1: Earthquakes for evaluation [18].

No.	M	Year	Record No.	Low freq. [Hz]	Name	PGA [g]	PGV [cm/s]
1-1	6.7	1994	953	0.25	NORTHR/MUL009 (Component1)	0.42	59
1-2	6.7	1994	953	0.25	NORTHR/MUL279 (Component2)	0.52	63
2-1	6.7	1994	960	0.13	NORTHR/LOS000 (Component1)	0.35	22
2-2	6.7	1994	960	0.13	NORTHR/LOS270 (Component2)	0.48	45
3-1	7.1	1999	1602	0.06	DUZCE/BOL000 (Component1)	0.73	56
3-2	7.1	1999	1602	0.06	DUZCE/BOL090 (Component2)	0.82	62
4-1	7.1	1999	1787	0.04	HECTOR/HEC000 (Component1)	0.27	29
4-2	7.1	1999	1787	0.04	HECTOR/HEC090 (Component2)	0.34	42
5-1	6.5	1979	169	0.06	IMPVALL/H-DLT262 (Component1)	0.24	26
5-2	6.5	1979	169	0.06	IMPVALL/H-DLT352 (Component2)	0.35	33
6-1	6.5	1979	174	0.25	IMPVALL/H-E11140 (Component1)	0.36	34
6-2	6.5	1979	174	0.25	IMPVALL/H-E11230 (Component2)	0.38	42
7-1	6.9	1995	1111	0.13	KOBE/NIS000 (Component1)	0.51	37
7-2	6.9	1995	1111	0.13	KOBE/NIS090 (Component2)	0.50	37
8-1	6.9	1995	1116	0.13	KOBE/SHI000 (Component1)	0.24	38
8-2	6.9	1995	1116	0.13	KOBE/SHI090 (Component2)	0.21	28
9-1	7.5	1999	1158	0.24	KOCAELI/DZC180 (Component1)	0.31	59
9-2	7.5	1999	1158	0.24	KOCAELI/DZC270 (Component2)	0.36	46
10-1	7.5	1999	1148	0.09	KOCAELI/ARC000 (Component1)	0.22	18
10-2	7.5	1999	1148	0.09	KOCAELI/ARC090 (Component2)	0.15	40
11-1	7.3	1992	900	0.07	LANDERS/YER270 (Component1)	0.24	51
11-2	7.3	1992	900	0.07	LANDERS/YER360 (Component2)	0.15	30

Table 2: Earthquakes for evaluation [18].

No.	M	Year	Record No.	Low freq. [Hz]	Name	PGA [g]	PGV [cm/s]
12-1	7.3	1992	848	0.13	LANDERS/CLW-LN (Component1)	0.42	42
12-2	7.3	1992	848	0.13	LANDERS/CLW-TR (Component2)	0.28	28
13-1	6.9	1989	752	0.13	LOMAP/CAP000 (Component1)	0.53	35
13-2	6.9	1989	752	0.13	LOMAP/CAP090 (Component2)	0.44	29
14-1	6.9	1989	767	0.13	LOMAP/G03000 (Component1)	0.56	36
14-2	6.9	1989	767	0.13	LOMAP/G03090 (Component2)	0.37	45
15-1	7.4	1990	1633	0.13	MANJIL/ABBAR-L (Component1)	0.52	42
15-2	7.4	1990	1633	0.13	MANJIL/ABBAR–T (Component2)	0.50	41
16-1	6.5	1987	721	0.13	SUPERST/B-ICC000 (Component1)	0.36	46
16-2	6.5	1987	721	0.13	SUPERST/B-ICC090 (Component2)	0.26	41
17-1	6.5	1987	725	0.25	SUPERST/B-POE270 (Component1)	0.45	36
17-2	6.5	1987	725	0.25	SUPERST/B-POE360 (Component2)	0.36	33
18-1	7	1992	829	0.07	CAPEMEND/RIO270 (Component1)	0.39	44
18-2	7	1992	829	0.07	CAPEMEND/RIO360 (Component2)	0.55	42
19-1	7.6	1999	1244	0.05	CHICHI/CHY101-E (Component1)	0.35	71
19-2	7.6	1999	1244	0.05	CHICHI/CHY101-N (Component2)	0.44	115
20-1	7.6	1999	1485	0.05	CHICHI/TCU045-E (Component1)	0.50	13
20-2	7.6	1999	1485	0.05	CHICHI/TCU045-N (Component2)	0.36	21
21-1	6.6	1971	68	0.25	SFERN/PEL090 (Component1)	0.21	19
21-2	6.6	1971	68	0.25	SFERN/PEL180 (Component2)	0.17	15
22-1	6.6	1976	125	0.13	FRIULI/A-TMZ000 (Component1)	0.35	22
22-2	6.6	1976	125	0.13	FRIULI/A-TMZ270 (Component2)	0.32	31

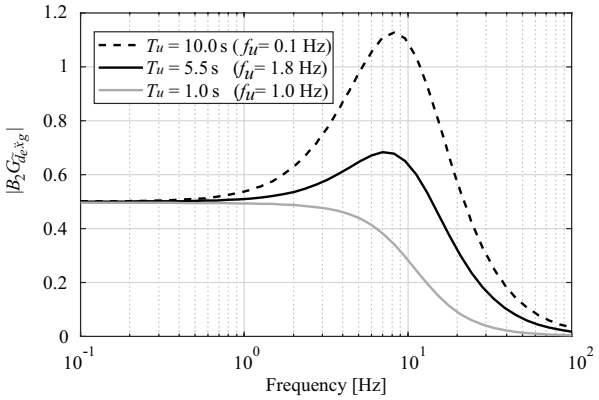

Fig. 9: Frequency response of $B_2 G_{\tilde{d}_e \ddot{x}_g}$ for T_u = 1.0, 5.5, and 10.0 s.

Table 3: Effect of parameter tuning of natural frequency of observer.

	avg $\left[\ddot{x}(t) + \ddot{x}_g(t)\right]$	avg $[\lvert u(t)\rvert_{\max}]$	std $\left[\ddot{x}(t) + \ddot{x}_g(t)\right]$	std $[\lvert u(t)\rvert_{\max}]$
f_o = 10 Hz	113.07	113.07	22.42	22.41
f_o = 3 Hz	87.73	89.48	16.25	16.00

Figure 10 shows the frequency response of $B_2 G_{\tilde{d}_e \ddot{x}_g}(s)$ for T_u = 10.0 s and the results of the Fourier transforms of PEL180 and CHY101-N waves (Nos. and 12 in Table 1, respectively). Since the gain of $B_2 G_{\tilde{d}_e \ddot{x}_g}(s)$ has a large peak around the frequency 8 Hz and is about 0.5 at a frequency lower than 1 Hz, the EID estimator can satisfactorily estimate vibrations caused by CHY101-N that has the dominant component of 0.2 Hz. However is not able to estimate those caused by PEL180 that has a main component at around 10 Hz (Fig. 10). This result is reflected in Fig. 11 (a) and (b). The EID for the CHY101-N was estimated with high accuracy. However, it is hard to estimate the EID for the PEL180, and the amplitude of the estimated EID, $\tilde{d}_e(t)/m$, is much higher than that of the actual EID, $N_F \ddot{x}_g(t)$. It is clear from the above observation that the estimation accuracy for the spectra can be improved by suitably designing the EID estimator. More specifically, the key is to design the EID estimator that ensures $|BG_{\tilde{d}_e \ddot{x}_g}(j\omega)| \approx N_F$ in the frequency range for disturbance estimation and rejection and if the peak is not much bigger than N_F.

Figure 12 shows the frequency response of $B_2 G_{FF}(s)$ for T_u = 10.0 s for the observer with different natural frequency f_o. It shows that the larger f_o is, the bigger the peak is. Since the selection of f_o = 3.0 Hz for the observer does not have a peak in 10 ∼ 100 Hz. Thus, we select it for T_u = 5.5 ∼ 10.0 s. A comparison before and after the tuning of the natural frequency of the observer for Figs. 8 and 13 (Table 3) shows that suitable tuning of f_o ensures that the estimates agree with the time-history analyses roughly in the range ±20%. Thus, the spectra can be used to estimate the maximum responses and shear force for suitably designed EID-based structural-control system. On the other hand, the spectra can be used to design a suitable EID-based structural-control system. From this viewpoint, we presented the algorithm of designing an EID-based structural-control system in Subsection 4.4.

5.2. Design example

An example for the control algorithm is shown to illustrate how the spectra are employed to select the parameters of an EID-based structural control system. First, for a structure

$$T_u = 3.0 \text{ s}, \ h_S = 0.02, \tag{76}$$

set

$$x_{lim} = 30 \text{ cm}, \ u_{lim}/mg = 0.25. \tag{77}$$

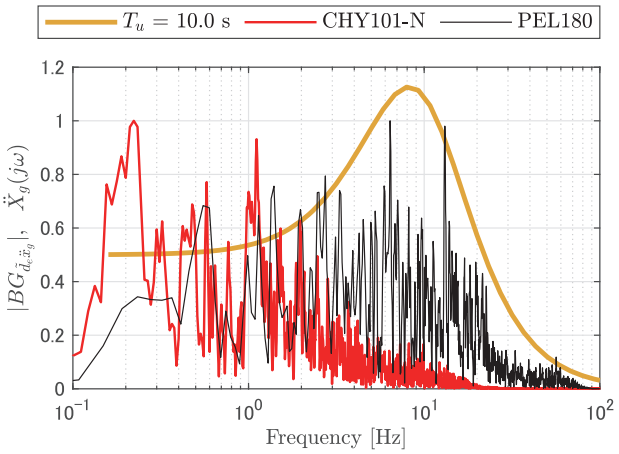

Fig. 10: Frequency response of $B_2G_{\tilde{d}_e\ddot{x}_g}(s)$ for $T_u = 10.0$ s and Fourier transform of PEL180 and CHY101-N.

Considering that the natural period of the building model is 3.0 s, we chose the maximum frequency for earthquake suppression to be

$$\omega_m = 20 \text{ rad/s}, \tag{78}$$

and set

$$T_F = 100 \text{ s},\ N_F = 0.5. \tag{79}$$

Next, we select CHY101-N for the design of the EID-based structural-control system, and the candidates for target control performance for the velocity-feedback controller to be

$$h_{Seq} = 0.4,\ 0.6,\ 0.8. \tag{80}$$

Calculating the velocity feedback controller using (67) yields

$$\begin{cases} K_P = \begin{bmatrix} 0 & -159.2 \end{bmatrix} \text{ for } h_{Seq} = 0.4, \\ K_P = \begin{bmatrix} 0 & -242.9 \end{bmatrix} \text{ for } h_{Seq} = 0.6, \\ K_P = \begin{bmatrix} 0 & -326.7 \end{bmatrix} \text{ for } h_{Seq} = 0.8. \end{cases} \tag{81}$$

Then, we used

$$f_o = 10, 30, 100 \text{ Hz},\ h_o = 0.8 \tag{82}$$

to construct an EID-based structural-control system.

The control performance of the control system is checked using the spectra [Fig. 14 (a)-(d)]. These spectra show that the maximum displacement is 31.0 cm and the C_U is 0.145 for the selection of $h_{Seq} = 0.8$, that is, the displacement is not satisfied the limitations given in (77).

The frequency responses of $B_2G_{\tilde{d}_e\ddot{x}_g}(s)$ for

$$f_o = 10 \text{ Hz} \tag{83}$$

shows that the gain does not have a peak and is almost 1 for the frequency up to 10 Hz (Fig. 15).

Finally, the spectra of the designed EID-based structural-control system [Fig. 16 (a)-(d)] show that the system satisfies all the limitations, has adequate control performance for the displacement, velocity, and absolute acceleration, and has a small control force.

Table 4 compares the spectra and the time-history analysis. It shows that the errors between the spectra and the time-history analyses are small and the presented spectra are able to be used to design an EID-based structural-control system. The control result for CHY101-N earthquake wave is shown in Fig. 17. The results for the feedback

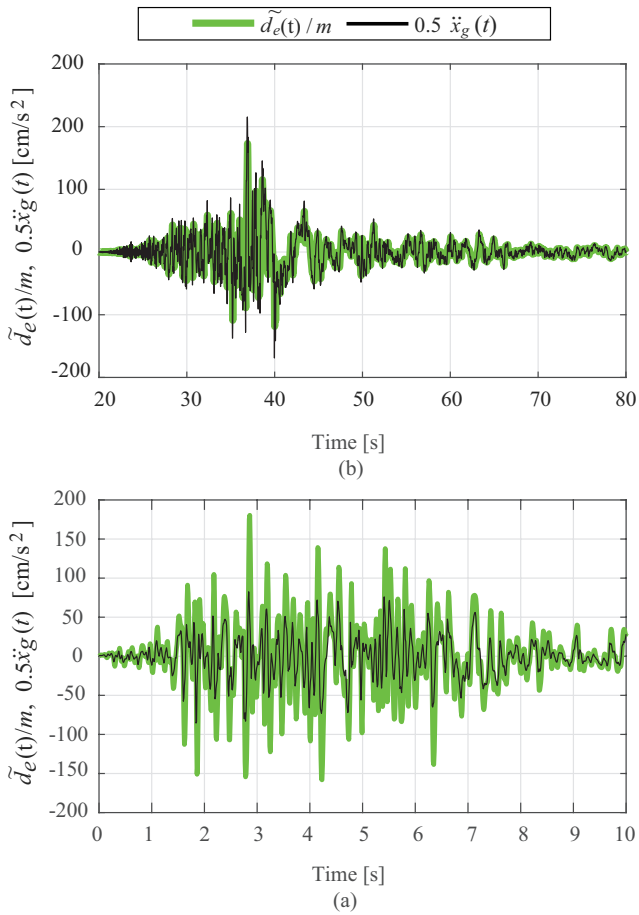

Fig. 11: Earthquake waves and EID estimates: (a) CHY101-N and EID and (b) PEL180 and EID.

control(without EID estimator) and no control (NC) are also shown in the same figure for comparison. The control results show that the control performance of the EID-based structural-control system, which was designed based on the presented spectra, for the displacement, the velocity, and the absolute acceleration are all better than that of the conventional LQR method.

Table 4: Comparison between spectra and time-history analyses (THA).

	Spectrum	Time history analysis (THA)	$\frac{\text{THA} - \text{Spectrum}}{\text{THA}} \times 100\%$
$x(t)$ [cm]	18.6	18.6	0%
$\dot{x}(t)$ [cm/s]	34.9	34.9	0%
$\ddot{x}(t) + \{1\}\ddot{x}_g(t)$ [cm/s^2]	226.7	204.5	10.9%
$u(t)/mg$	0.22	0.23	5%

6. Conclusion

This paper presented new spectra of response and control force for an equivalent-input-disturbance (EID)-based structural-control system that contains both feedforward and feedback terms from disturbances to a control output. While the EID approach yielded better control performance than conventional control methods, sophisticated tuning

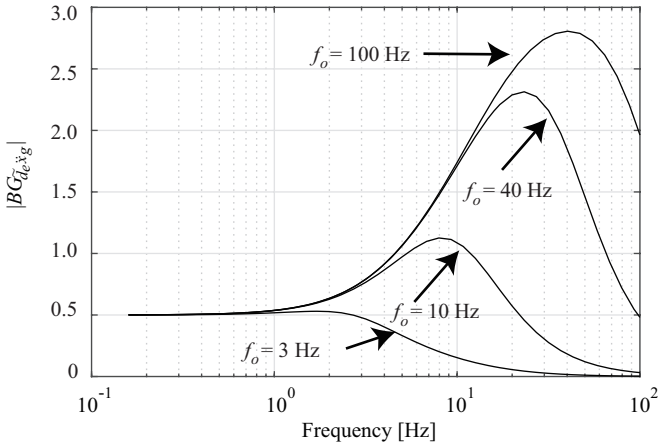

Fig. 12: Frequency response of $B_2 G_{\ddot{d}_e \ddot{x}_g}(s)$ for $T_u = 10.0$ s.

of control parameters in the system is a hard task. The spectra were used to simplify the design of the system. This paper clarified the following points:

- We derived the configuration of the system from disturbances to a control output for the EID-based structural-control system. Then, we devised new spectra of the displacement, the velocity, the absolute acceleration, and the control force to precisely describe such relationships.
- We illustrated how to use the spectra to simplify the design of an EID-based structural-control system, and presented a designing algorithm based on the spectra. Design rules explained in the algorithm make use of frequency responses. This makes the design process visible and easy to understand.
- The validity of the use of the spectra was demonstrated through the structural control of a shear building model for 44 kinds of earthquake waves.

Note that the spectra were used in the design of an EID-based structural-control system in this study. It can be applied directly to other disturbance-rejection methods that contain disturbance-estimation mechanisms, such as the disturbance observer and the active disturbance-rejection control.

In addition, although the response spectrum method easily estimates the peak value of the response of a linear system, most structures contain nonlinearities. Investigation of the influence of nonlinearities is of great importance and can provide a theoretical guarantee of the control performance of a designed system, and will be carried out in the future.

This study dealt with an SDOF model. In the next stage of our research, we planned to apply our method to an MDOF model.

Appendix A. Derivation of transfer function C_{FF} in (19)

(3) and (10) yield

$$\begin{cases} \Delta\dot{z}(t) = (A - L_P C)\Delta z(t) + B_d \ddot{x}_g(t) \\ \Delta y(t) = C\Delta z(t). \end{cases} \tag{A.1}$$

The transfer function from $\ddot{x}_g(t)$ to $\Delta z(t)$ is

$$G_{\Delta y \ddot{x}_g} = \frac{\Delta Z(s)}{\ddot{X}_g(s)} = C(sI - A + L_P C)^{-1} B_d, \tag{A.2}$$

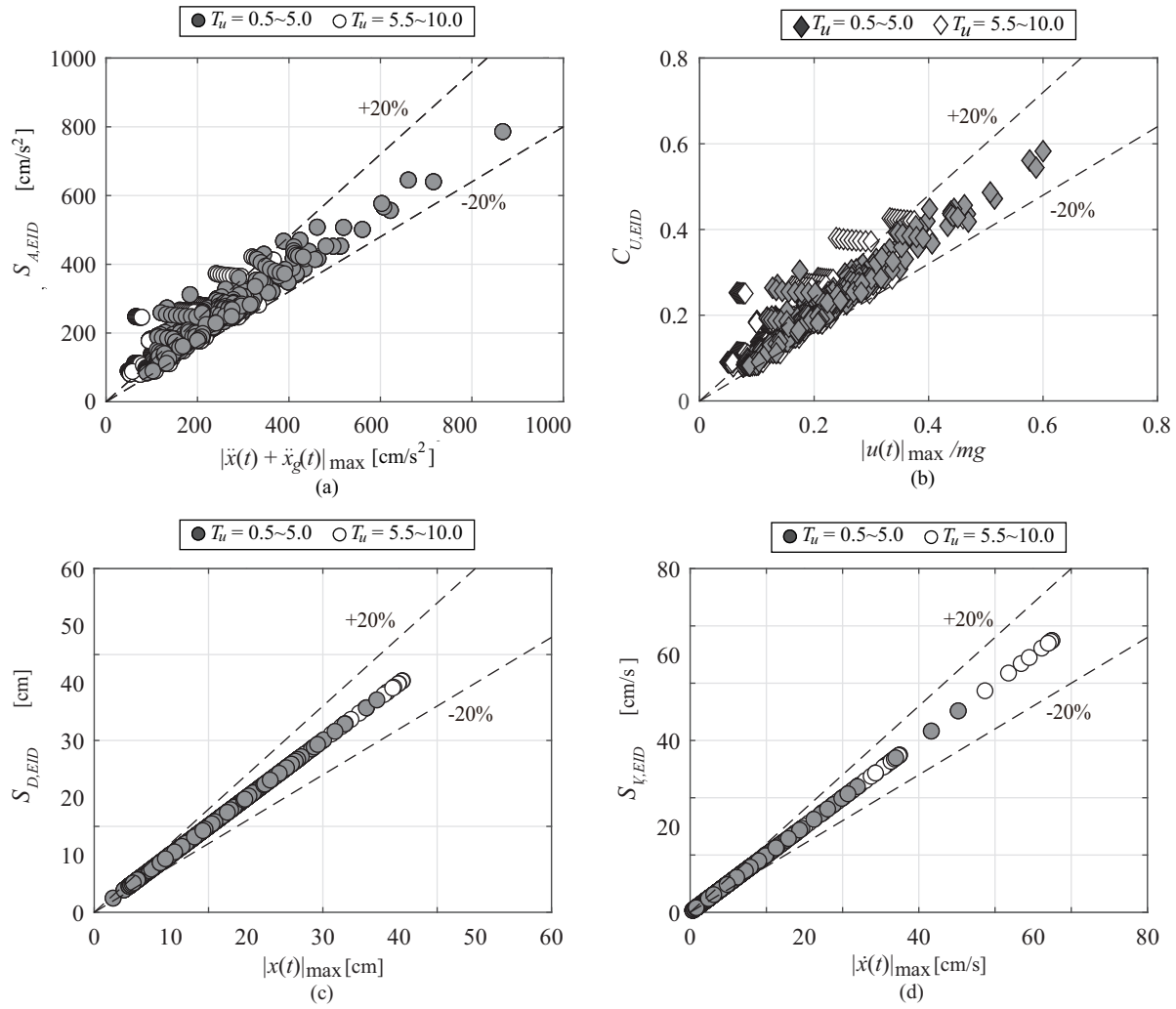

Fig. 13: Estimation vs. analysis for (a) maximum absolute acceleration, (b) maximum C_U (N_F = 0.5), (c) displacement, and (d) velocity for f_o = 3 Hz.

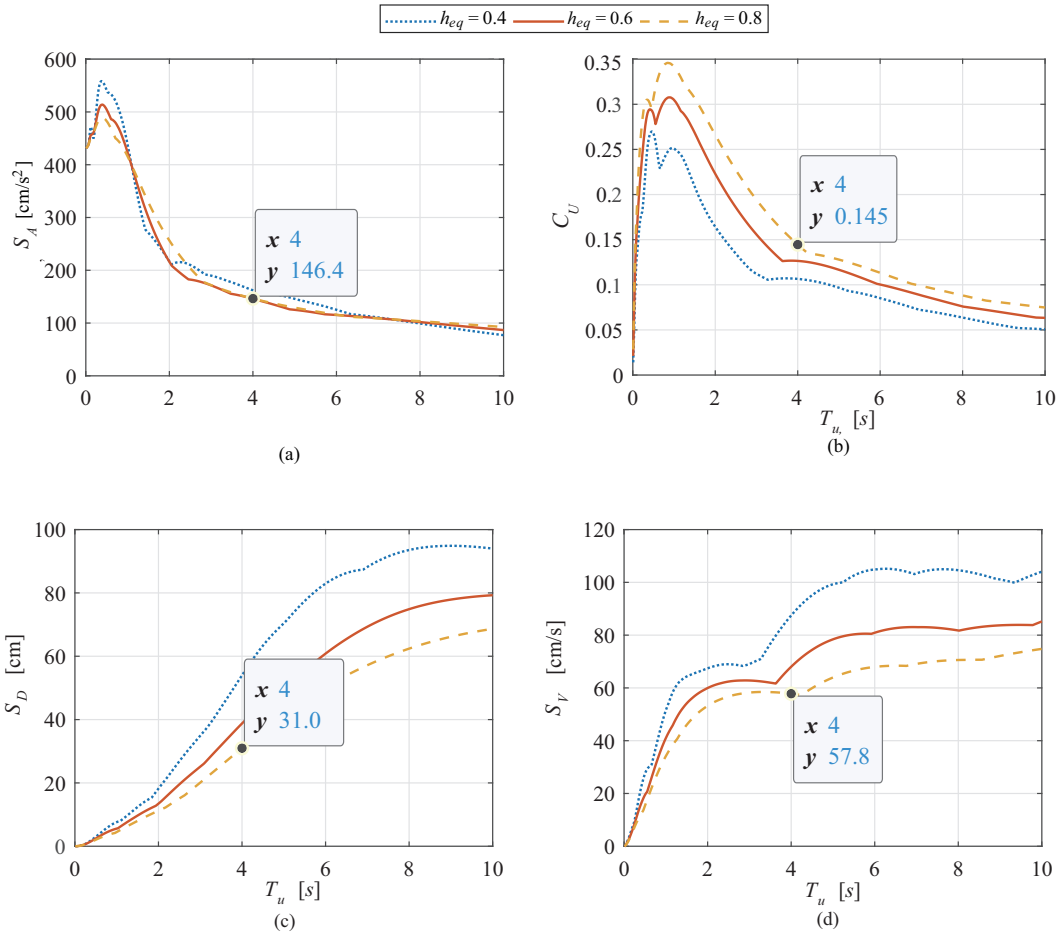

Fig. 14: Response spectra of (a) displacement, (b) velocity, (c) absolute acceleration, and (d) C_U.

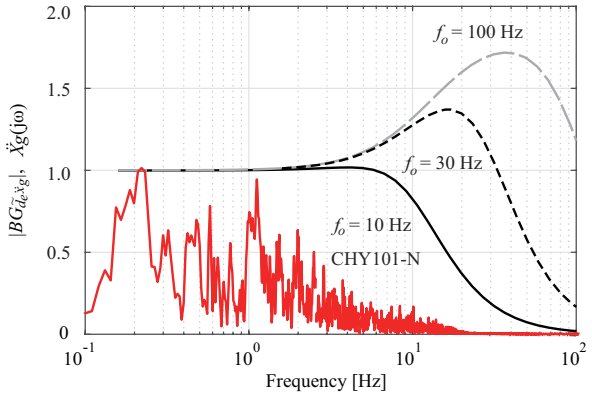

Fig. 15: Frequency responses of $B_2G_{\tilde{d}_e\ddot{x}_g}(s)$ for (82).

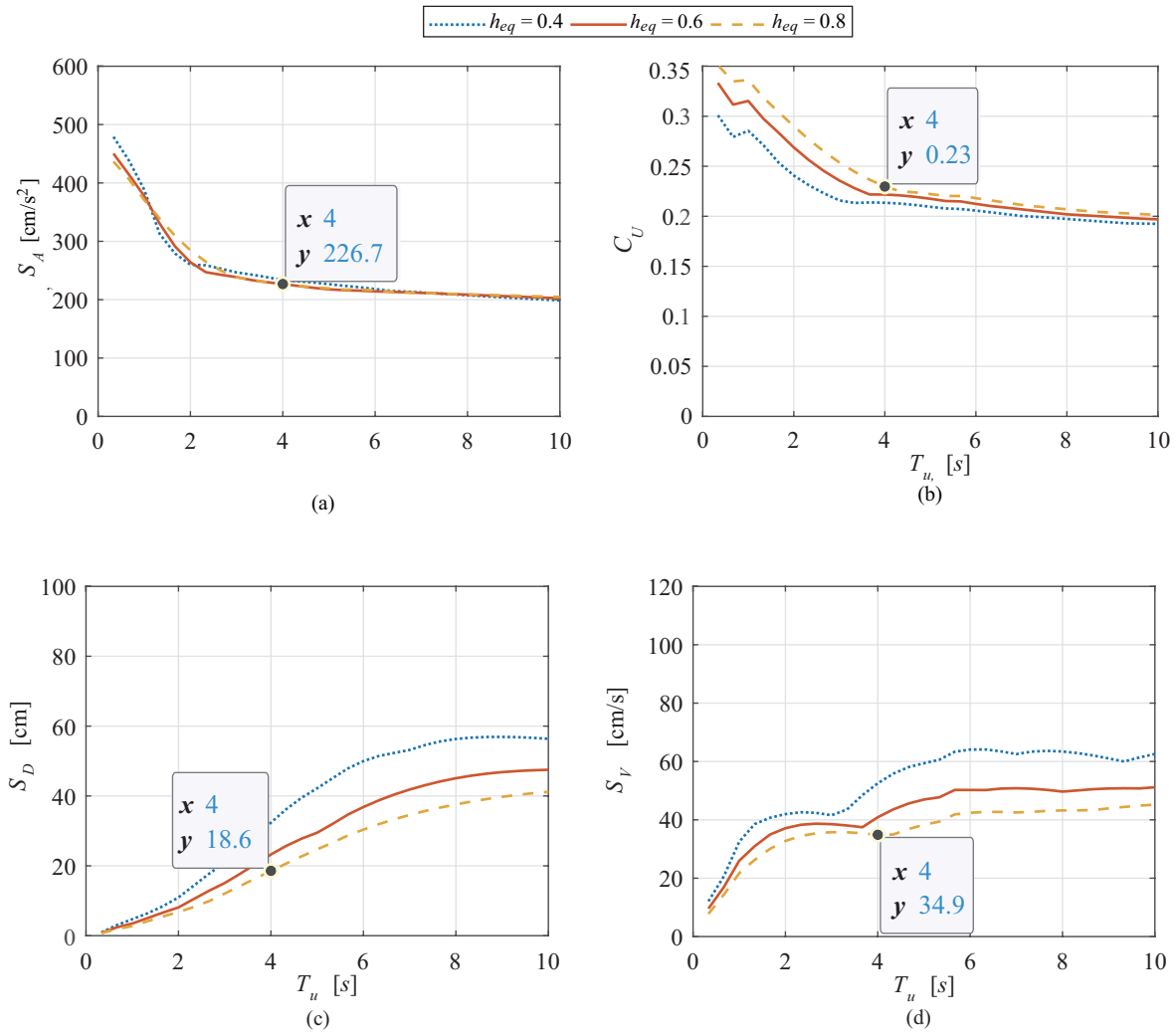

Fig. 16: Response spectra for EID-based structural-control system: (a) displacement, (b) velocity, (c) absolute acceleration, and (d) C_U.

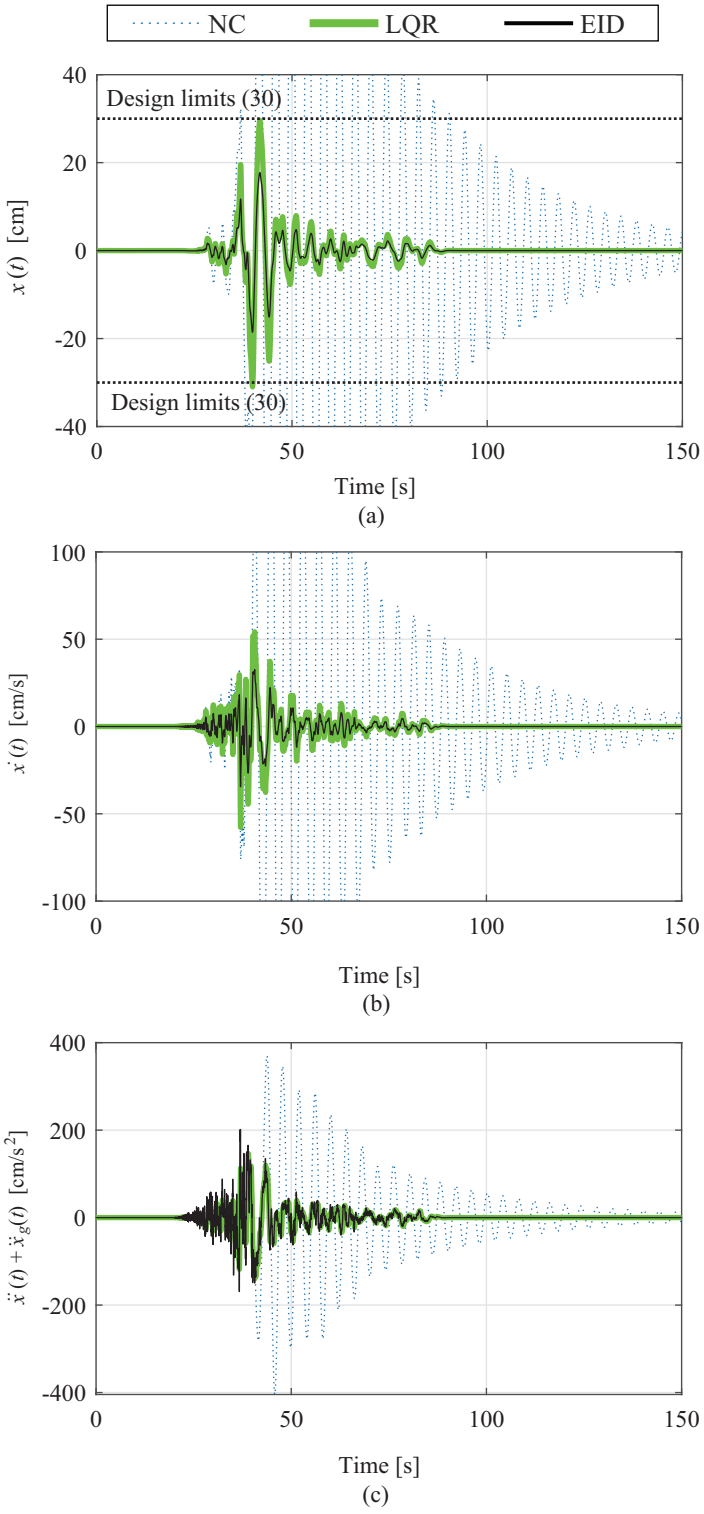

Fig. 17: Time responses for EID, LQR, and NC: (a) displacement, (b) velocity, and (c) absolute acceleration.

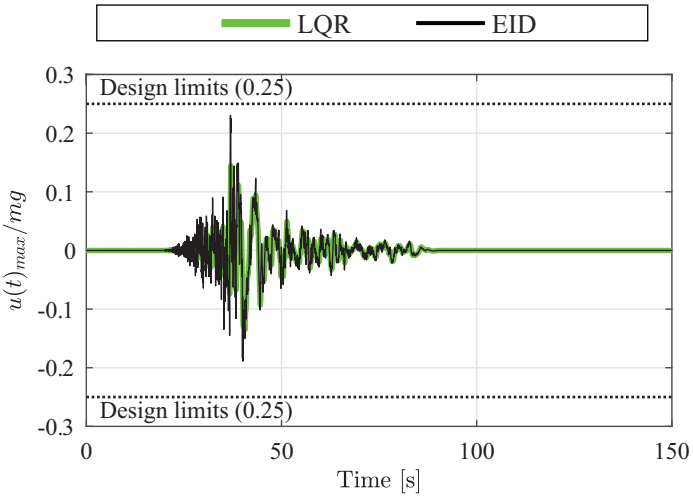

Fig. 18: Control input for EID and LQR.

where $\ddot{X}_g(s)$ and $\Delta Z(s)$ are Laplace transform of $\ddot{x}_g$ and $\Delta z(t)$ respectively. Combining the (A.2), (15), and the Laplace transform of (13) yields the estimated EID $\tilde{D}_e(s)$:

$$\tilde{D}_e(s) = F(s)B^+ L_P G_{\Delta y \ddot{x}_g}(s)\ddot{X}_g(s). \tag{A.3}$$

On the other hand, combining the equations (3), (16), and (17) gives

$$\dot{z}(t) = (A + BK_P)z(t) + B_d\ddot{x}_g(t) - B\tilde{d}_e(t). \tag{A.4}$$

The Laplace transform of (A.4) yields

$$sZ(s) = (A + BK_P)Z(s) + B_d\ddot{X}_g(s) - B\tilde{D}_e(s). \tag{A.5}$$

Substituting (A.3) into (A.5), we have

$$sZ(s) = (A + BK_P)Z(s) + (B_d - F(s)B^+ L_P G_{\Delta y \ddot{x}_g})\ddot{X}_g(s). \tag{A.6}$$

The transfer function from $\ddot{X}_g(s)$ to $Z(s)$, $G_z(s)$ is

$$\begin{aligned} G_{z\ddot{x}_g}(s) &= \frac{Z(s)}{\ddot{X}_g(s)} \\ &= (sI - A - BK_P)^{-1}(B_d - F(s)B^+ L_P G_{\Delta y \ddot{x}_g}(s)). \end{aligned} \tag{A.7}$$

Then, $B_d - BF(s)B^+ L_P G_{\Delta y \ddot{x}_g}(s)$ is the transfer function of the feedforward term, $G_{FF}(s)$.

Appendix B. Velocity response spectra of FENA waves

The velocity response spectra for 5% damping ratio of the earthquake waves in Tabs. 5.1 and 5.1 are shown (Figs. B.19-B.40). These figures show that these waves cover a wide range of frequency band.

References

[1] The Japan Society of seismic isolation, Recent trends in seismic isolation buildings, 2017 (http://www.jssi.or.jp/menshin/doc/keizoku2.pdf) [in Japanese]

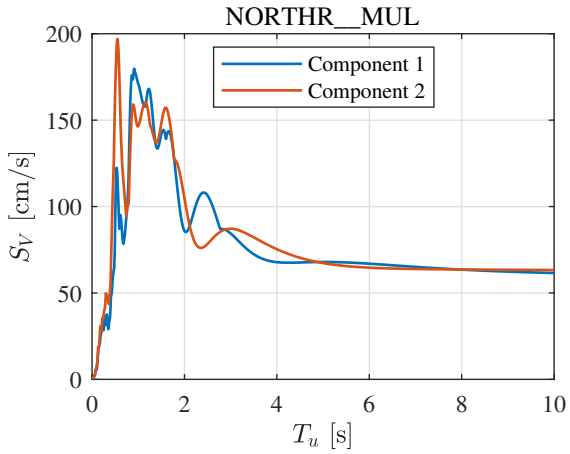

Fig. B.19: Velocity response of NORTHR/MUL009 and MUL279

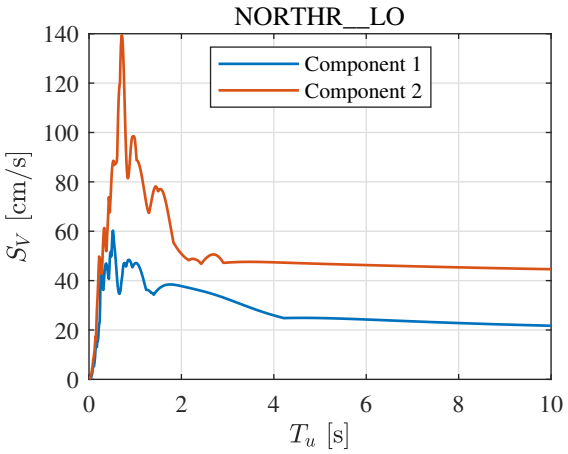

Fig. B.20: Velocity response of NORTHR/LOS000 and LOS270

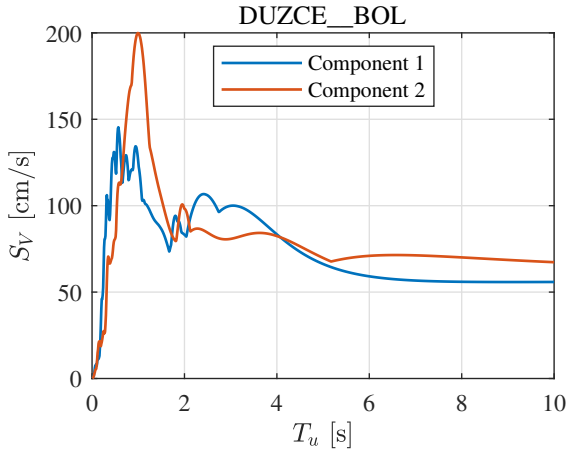

Fig. B.21: Velocity response of DUZCE/BOL000 and BOL090

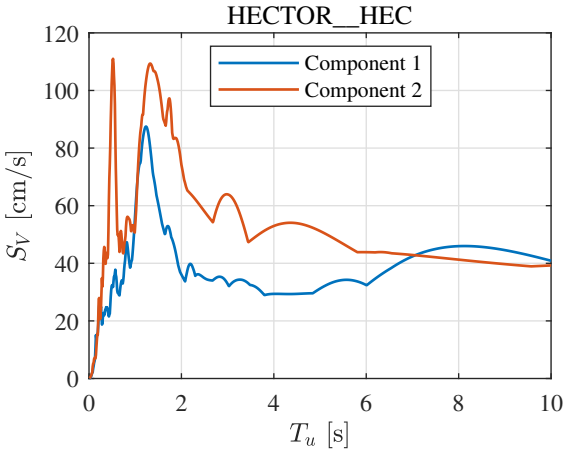

Fig. B.22: Velocity response of HECTOR/HEC000 and HEC090

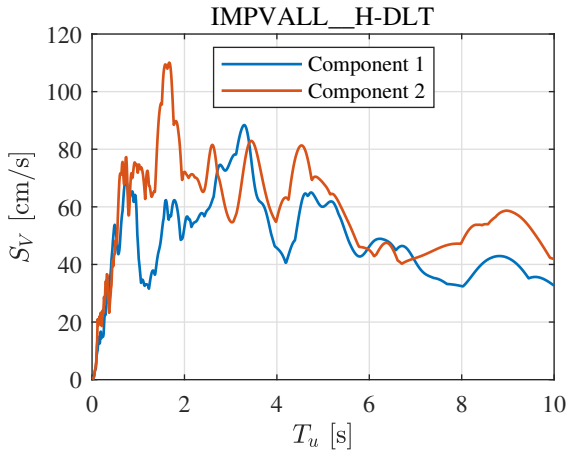

Fig. B.23: Velocity response of IMPVALL/H-DLT262 and H-DLT352

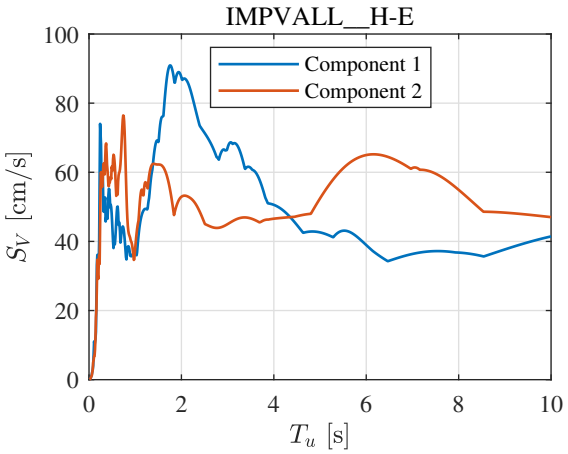

Fig. B.24: Velocity response of IMPVALL/H-E11140 and H-E11230

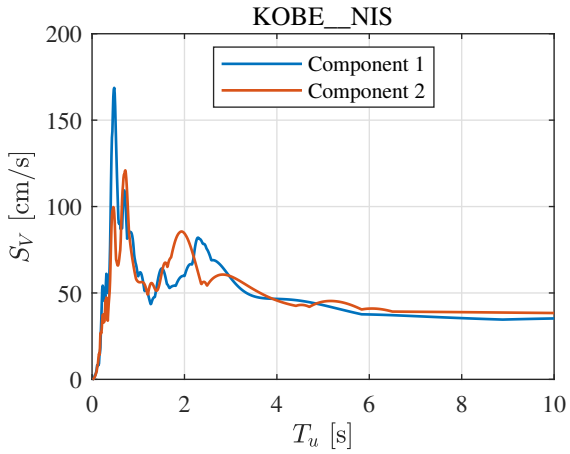

Fig. B.25: Velocity response of KOBE/NIS000 and NIS090

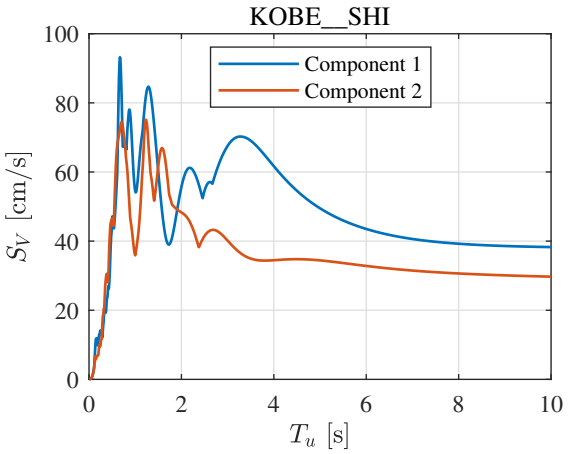

Fig. B.26: Velocity response of KOBE/SHI000 and SHI090

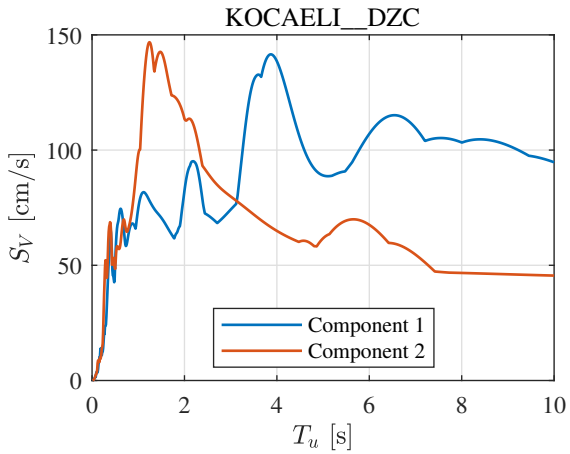

Fig. B.27: Velocity response of KOCAELI/DZC180 and DZC270

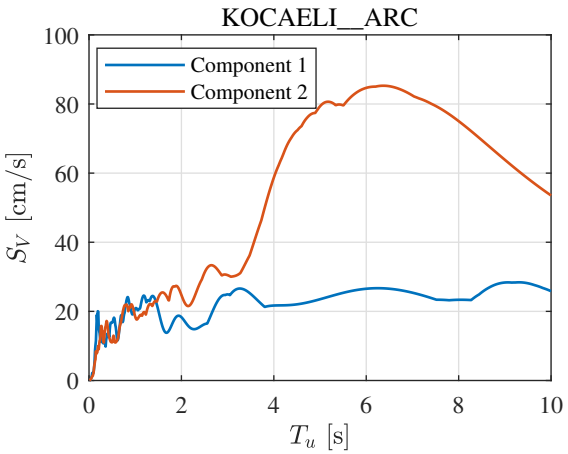

Fig. B.28: Velocity response of KOCAELI/ARC000 and ARC090

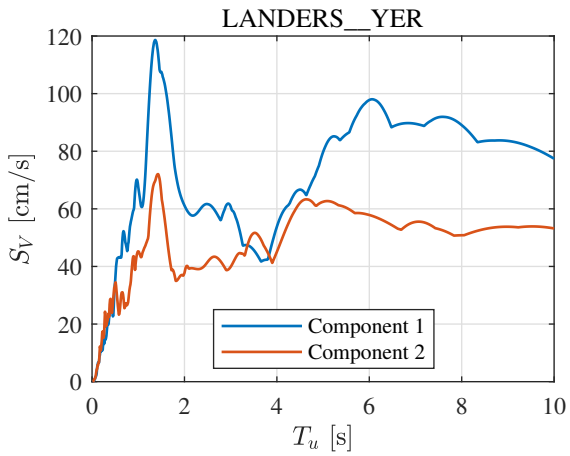

Fig. B.29: Velocity response of LANDERS/YER270 and YER360

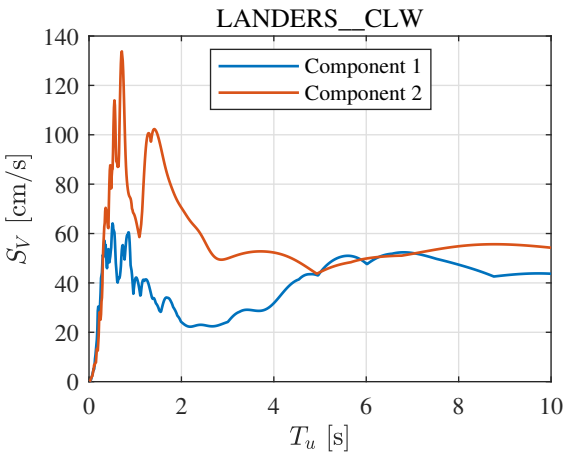

Fig. B.30: Velocity response of LANDERS/CLW-LN and CHY101-N

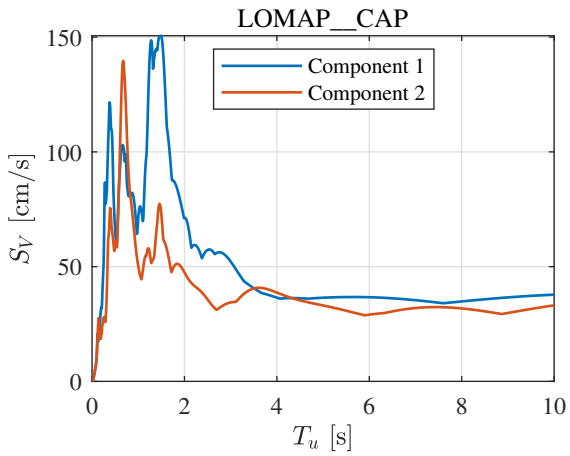

Fig. B.31: Velocity response of LOMAP/CAP000 and CAP090

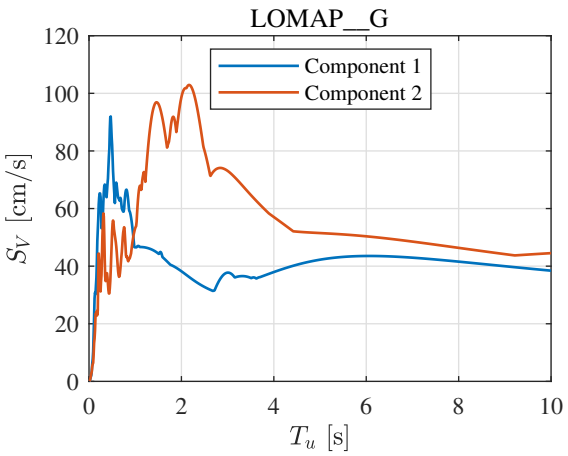

Fig. B.32: Velocity response of LANDERS/G03000 and G03090

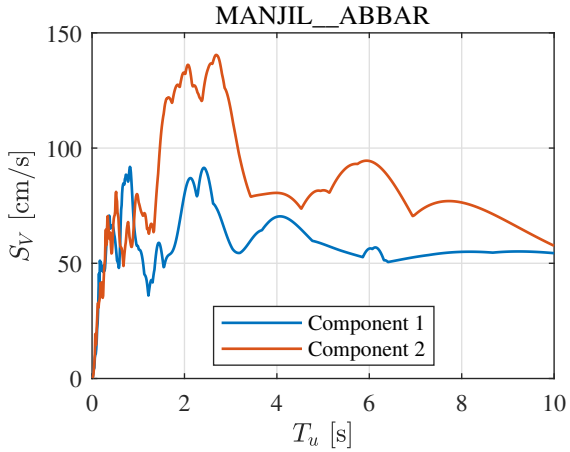

Fig. B.33: Velocity response of MANJIL/ABBAR-L and ABBAR

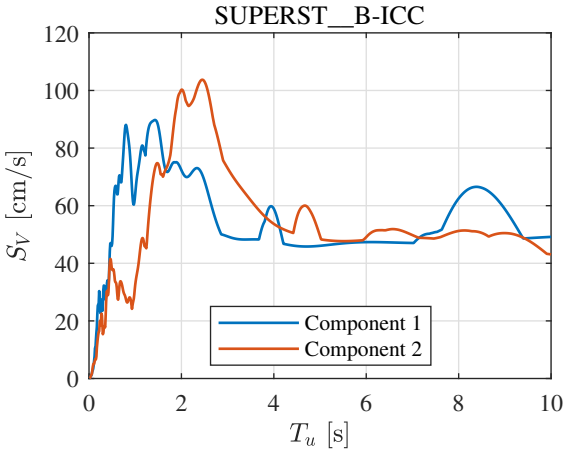

Fig. B.34: Velocity response of SUPERST/B-ICC000 and B-ICC090

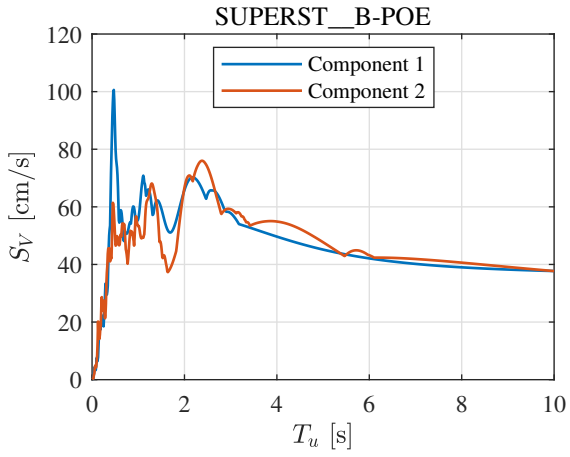

Fig. B.35: Velocity response of SUPERST/B-POE270 and B-POE360

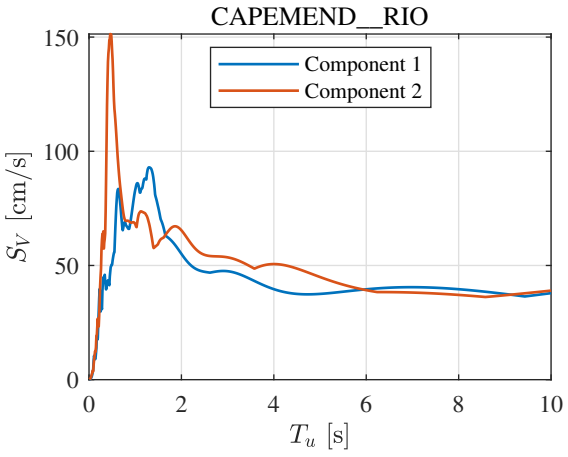

Fig. B.36: Velocity response of CAPEMEND/RIO270 and RIO360

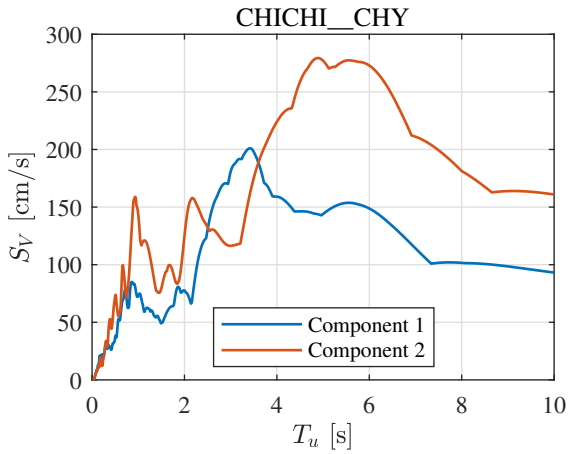

Fig. B.37: Velocity response of CHICHI/CHY101-E and CHY101-N

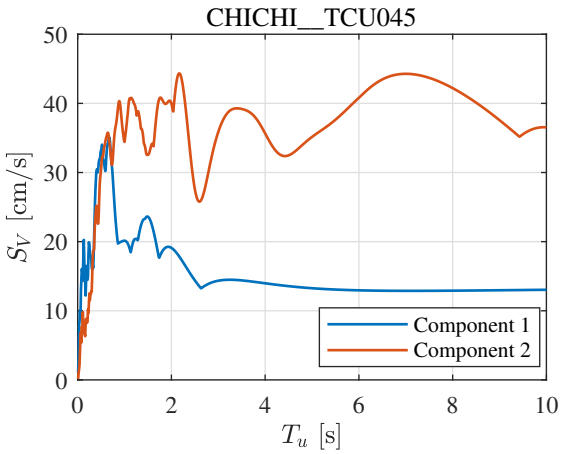

Fig. B.38: Velocity response of CHICHI/TCU045-E and TCU045-N

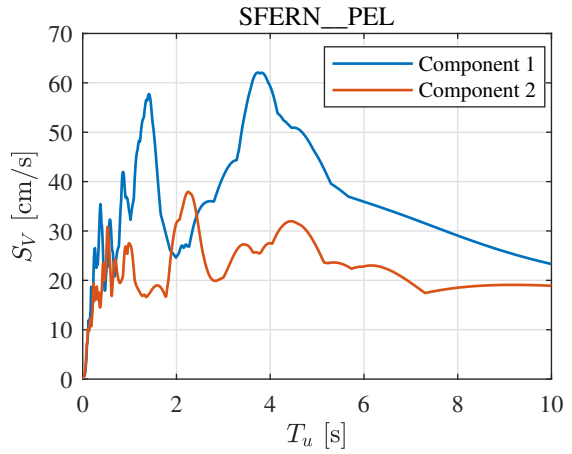

Fig. B.39: Velocity response of SFERN/PEL090 and PEL180

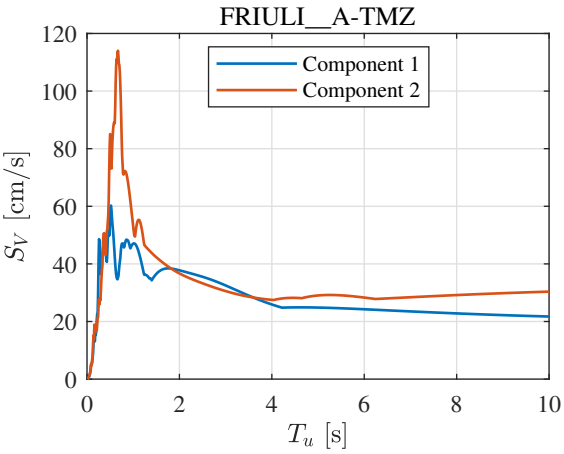

Fig. B.40: Velocity response of FRIULI/A-TMZ000 and A-TMZ270

[2] S. Thenozhi and W. Yu, Stability analysis of active vibration control of building structures using PD/PID control, *Engineering Structures*, 81 (2016) 208-218.
[3] E. Talib, J.-H. Shin, and M. K. Kwak, Designing multi-input multi-output modal-space negative acceleration feedback control for vibration suppression of structures using active mass dampers, *Journal of Sound and Vibration*, 439 (20) (2019) 77-98.
[4] X. Gu., Y. Yu, J. Li, and Y. Li, Semi-active control of magnetorheological elastomer base isolation system utilizing learning-based inverse model, *Journal of Sound and Vibration*, 406 (2017) 346-362.
[5] K. Miyamoto, J. She, J. Imani, X. Xin, and D. Sato, Equivalent-input-disturbance approach to active structural control for seismically excited buildings, *Engineering Structures*, 125 (2016) 392-399.
[6] K.-S. Park, H.-M. Koh, and S.-Y. Ok, Active control of earthquake excited structures using fuzzy supervisory technique, *Advances in Engineering Software*, 33 (11.12) (2002) 761-768.
[7] H. C. Cho, S. Fadali, M. Saiid, and K. S. Lee, Neural network active control of structures with earthquake excitation, *International Journal of Control Automation and Systems*, 3 (2) (2005) 202-210.
[8] I. Hashlamon, Adaptive Disturbance Estimation and Compensation for Delta Robots,*Jordan Journal of Mechanical and Industrial Engineering*, 14(4) (2020) 413-422.
[9] K. Ohishi, M. Nakano, K. Ohnishi, and K, Miyachi, Microprocessor controlled DC motor for load insensitive position servo system, *IEEE Trans. Ind. Electron.*, 34 (1) (1987) 339-344.
[10] Q. Zheng and Z. Gao, Active disturbance rejection control: some recent experimental and industrial case studies, *Control Theory and Technology*, 16 (4) (2018) 301-313.
[11] J. She, M. Fang, Y. Ohyama, H. Hashimoto, and M. Wu, Improving disturbance rejection performance based on an equivalent-input-disturbance approach, *IEEE Transaction of Industrial Electron.*, 55 (1) (2008) 380-389.
[12] J. She, K. Sekiya, M. Wu, and Q. Lei, Active structural control with input dead zone based on equivalent-input-disturbance approach, *The 36th Annual Conference on IEEE Industrial Electronics Society (IECON 2010)*, (2010) 47-52.
[13] K. Miyamoto, J. She, and D. Sato, Active structural control with suppression of Absolute acceleration using equivalent-input-disturbance approach, *The 27th International Symposium on Industrial Electronics (ISIE 2018)*, (2018).
[14] K. C. Anil, *Dynamics of structures, Theory and applications to earthquake engineering*, 3rd edition (2006).
[15] Architectural of Institute of Japan, Design Recommendations for Seismically Isolated Buildings, *Transactions of AIJ*, Architectural of Institute of Japan (2016) (https://www.aij.or.jp/ppv/productId/428856/.)
[16] S. Pathak and V. K. Gupta, On nonstationarity-related errors in modal combination rules of the response spectrum method, *Journal of Sound and Vibration*, 407 (2017) 106-127.
[17] D. Sato, Y. Chen, K. Miyamoto, and J. She, A spectrum for estimation the maximum control force for passive-base-isolated with LQR control, *Engineering Structures*, 199 (15) (2019) (DOI: 10.1016/j.engstruct.2019.109600).
[18] Quantification of Building Seismic Performance Factors, FEMA P695 (2009), (https://www.fema.gov/media-library-data/20130726-1716-25045-9655/fema_p695.pdf).